AGU PUBLICATIONS

Geophysical Research Letters

Supporting Information for

Imaging the Hydrothermal System of Kirishima Volcanic Complex, Japan with L-band InSAR Time Series

Zhang Yunjun[1,†], Falk Amelung[1], Yosuke Aoki[2]

[1]Rosenstiel School of Marine and Atmospheric Science, University of Miami, Miami, Florida, USA

[2]Earthquake Research Institute, University of Tokyo, Tokyo, Japan

[†]Now at Seismological Laboratory, California Institute of Technology, Pasadena, California, USA

Corresponding author: Z. Yunjun (yunjunzgeo@gmail.com)

Contents of this file

Table S1 to S4.

Figure S1 to S24.

Introduction

Table S1 summarizes the used satellite SAR data information and configurations used in the InSAR stack processing. Table S2 summarizes the impact of the minimum free surface height on the estimated source parameters. Table S3 lists the configurations used for parameter optimization of geodetic modeling. Table S4 lists the parameter of the optimal solution from geodetic modeling with their 95% confidence intervals.

Fig. S1 shows the network configuration of interferometric pairs used in the stack processing. Fig. S2-S4 show the temporal coherence, estimated DEM errors and noise level in terms of residual phase root mean squares of the InSAR time series analysis.

Fig. S5-S8 show the displacement time-series of the Kirishima volcanic complex from the four orbits (ALOS and ALOS-2, ascending and descending) in the line-of-sight direction after all the phase corrections. Fig. S9-S10 show the displacement time-series of the Shinmoe-dake crater from ALOS-2 ascending and descending orbits estimated without interferograms after the 2017 Shinmoe-dake eruption.

Fig. S11 demonstrates the impact of the two extra steps after the MintPy routine workflow on the displacement estimation for time periods of interest. Fig. S12 shows the thickness of the lava dome extruded from the 2011 Shinmoe-dake eruption estimated using the DEM error.

Fig. S13-S15 show displacement map of Kirishima during the three representative time periods from ascending/descending and their decomposition in quasi-horizontal/vertical direction.

Fig. S16 shows the displacement due to ash/tephra deposition from the 2017 Shinmoe-dake eruption. Fig. S17 shows the pre-eruptive inflation, co-eruptive deflation and ash/tephra deposition from the 2011 Shinmoe-dake eruption.

Fig. S18-S19 show the subsampling result of InSAR displacement as the input of geodetic modeling. Fig. S20-S23 show the joint probability density distribution among all free parameters of the geodetic modeling. Fig. S24 shows the residual between the observed and predicted displacement from geodetic modeling for the expanded inflation at Iwo-yama after Dec 2017.

Satellite	*ALOS*		*ALOS-2*	
Orbit direction	*ascending*	*descending*	*ascending*	*descending*
Track	*424*	*73*	*131*	*23*
Frame	*620-630*	*2970-2980*	*620*	*2970*
Start date	*2006-06-24*	*2007-01-07*	*2014-09-30*	*2015-02-09*
End date	*2011-04-07*	*2011-04-20*	*2019-07-02*	*2019-08-19*
Number of acquisitions	*29*	*21*	*36*	*49*
Number of interferograms	*225*	*115*	*204*	*341*
Max perpendicular baseline [m]	*1800*	*1800*	*200*	*200*
Max temporal baseline [day]	*1800*	*1800*	*400*	*400*
# of looks in range direction	*4*	*4*	*8*	*8*
# of looks in azimuth direction	*10*	*10*	*10*	*10*
power spectral filter strength (Goldstein & Werner, 1998)	*0.5*	*0.5*	*0.5*	*0.5*

Table S1. *SAR dataset information with parameters used in InSAR stack processing. To form the ALOS interferograms, we oversample the SAR images which are acquired in fine beam dual-polarization mode with 14 MHz bandwidth to 28 MHz, the bandwidth of fine beam single polarization mode.*

Finite sphere (McTigue, 1987)								
Min free surface hgt. (MFSH) [m]	*Points below MFSH* *Perc.*	 *Height incr. [m] avg. [min, max]*	*Latitude [°]*	*Longitude [°]*	*Depth [m]*	*Radius [m]*	*ΔP/μ [10^{-2}]*	*ΔV [10^3m^3]*
None	*0%*	*0*	*31.9469* *± 0.0001*	*130.8531* *± 0.0001*	*150 (1162)* *± 10*	*40$^{\#}$* *± 7*	*4.3* *± 1.7*	*8.7* *± 1.1*
1250	*11%*	*49* *[0, 237]*	*31.9469* *± 0.0001*	*130.8531* *± 0.0001*	*150 (1162)* *± 10*	*40$^{\#}$* ± **8**	**4.4$^{\#}$** ± **1.9**	**8.8** *± 1.1*
1300	*59%*	*32* *[0, 287]*	**31.9468** *± 0.0001*	*130.8531* *± 0.0001*	**165** (**1148**) *± 10*	*40$^{\#}$* ± **17**	**5.7$^{\#}$** ± **5.5**	**11.8** ± **1.5**

CDM (Nikkhoo et al., 2016)											
MFSH [m]	*Latitude [°]*	*Longitude [°]*	*Depth [m]*	*ω_X [°]*	*ω_Y [°]*	*ω_Z [°]*	*a_X [m]*	*a_Y/a_X*	*a_Z/a_X*	*opening [m]*	*ΔV [10^3m^3]*
1250	*31.9470* *± 0.0001*	*130.8532* *± 0.0001*	*130 (1184)* *± 10*	*5* *± 2*	*-8* *± 2*	*0^{fix}*	*60* *± 10*	*1.2* *± 0.4*	*1.0* *± 0.2*	*0.28* *± 0.10*	*13* *± 2*
1300	*31.9470* *± 0.0001*	*130.8532* *± 0.0001*	*130 (*__1181__*)* *± 10*	*5* *± 2*	*-8* *± 2*	*0^{fix}*	*60* *± 10*	*1.2* ± **0.3**	**1.1** *± 0.2*	**0.30** ± **0.08**	**15** *± 2*

Table S2. *Impact of the minimum free surface height (MFSH) constraint on the source parameter estimation at Iwo-yama during 2015-2017 (Fig. 2k-o). We use both the finite sphere model (McTigue, 1987; does not require positive depths) and the CDM solution (Nikkhoo et al., 2016; do require positive depths) with different MFSH settings. Differences are highlighted in bold. Check Table S4 for detailed explanation of parameters and equations for volume change. Conclusions are:* **1)** *Between the finite sphere results without MFSH and with MFSH of 1250 m, the difference is negligible due to the low percentage (11%) of affected data points. Thus, we expect negligible impact at Shinmoe-dake during 2008-2010 and during 2015-2017 due to the similar low percentage (<=12%) and far-field locations (Fig. S18) of affected data points.* **2)** *Considering the similar CDM results with MFSH of 1250 m and of 1300 m, we conclude the impact of MFSH is negligible for Iwo-yama during 2015-2017.* **3)** *Comparing the finite sphere results without MFSH and with MFSH of 1300 m, the depth increase (15 m) is much smaller than the average height increase (32 m). Similarly, for Iwo-yama during 2015-2017 with the average height increase of 56 m for 77% of the data points (Fig. S19), we except less than 56 m of estimated depth increase, which is well within the reported 95% confidence interval of 100 m.*

Shinmoe-dake					
		2008-2010		2015-2017	
		ascending	descending	ascending	descending
Reference point [°]		[130.88; 31.91]			
Bounding box in WNES [°]		[130.85; 31.94; 130.91; 31.88]			
Remove constant offset Remove ramp		yes no		yes no	
Structural function	sill [m^2]	3.7e-05	2.8e-05	5.0e-05	4.4e-05
	range [m]	1300	2100	1460	940
	nugget [m]	1.1e-06	6.7e-06	6.8e-06	7.3e-06
Quadtree sampling	max var [m^2]	0.002^2	0.0025^2	0.0035^2	0.0035^2
	end level	15	15	7	7
	min pixel #	3	3	15	15
	WNES [°]	[130.865; 31.925; 130.900; 31.900]		[130.865; 31.925; 130.900; 31.900]	
Grid sampling	step [m]	750		1500	
min free surface height [m]		1100		1100	
Iwo-yama					
		2015-2017		2017-2019	
		ascending	descending	ascending	descending
Reference point [°]		[130.853; 31.947]			
Bounding box in WNES [°]		[130.832; 31.960; 130.870; 31.935]			
Remove constant offset Remove ramp		yes no		yes yes	
Structural function	sill [m^2]	3.6e-05	3.1e-05	9.5e-05	13e-05
	range [m]	1060	860	1800	2100
	nugget [m]	8.0e-06	6.7e-06	5.9e-06	6.6e-07
Quadtree sampling	max var [m^2]	0.006^2	0.0075^2	0.0045^2	0.0040^2
	end level	15	15	9	9
	min pixel #	1	1	2	2
	WNES [°]	[130.842; 31.954; 130.862; 31.941]		[130.840; 31.954; 130.862; 31.940]	
Grid sampling	step [m]	600		600	
min free surface height [m]		1300		1300	

Table S3. *Configurations for parameters optimization used in the GBIS software. Related to section 6. Sill, range and nugget are the three parameters used to describe the exponential fit to the experimental variogram calculated from the InSAR observation.*

Time period	Latitude [°]	Longitude [°]	Depth [m]	ω_X [°]	ω_Y [°]	ω_Z [°]	a_X [m]	a_Y/a_X	a_Z/a_X	opening [m]	ΔV [$10^3 m^3$]	Source shape
Shinmoe-dake (1,421 m a.s.l.)												
2008-2010	*31.9125 ± 0.0006*	*130.8845 ± 0.0004*	*620 (800) ± 50*	*-19 ± 12*	*12 ± 9*	*18 ± 15*	*190 ± 80*	*0.8 ± 0.7*	*1.4 ± 0.7*	*-0.26 ± 0.15*	*-124 ± 26*	*prolate ellipsoid*
2015- 2017	*31.9111 ± 0.0011*	*130.8828 ± 0.0013*	*730 (693) ± 210*	0^{fix}	0^{fix}	0^{fix}	*200*[#] *± 100*	1^{fix}	1^{fix}	*0.30 ± 0.19*	*146 ± 95*	*sphere*
Iwo-yama (1,313 m a.s.l.)												
2015- 2017	*31.9470 ± 0.0001*	*130.8532 ± 0.0001*	*130 (1181) ± 10*	*5 ± 2*	*-8 ± 2*	0^{fix}	*60 ± 10*	*1.2 ± 0.5*	*1.1 ± 0.2*	*0.30 ± 0.08*	*15 ± 2*	*sphere*
2017-2019	*31.9464 ± 0.0003*	*130.8530 ± 0.0002*	*340 (970) ± 100*	0^{fix}	0^{fix}	0^{fix}	*380 ± 80*	*0.3 ± 0.3*	*0.2 ± 0.4*	*0.16*[#] *+ 0.14 ± 0.08*	*76 ± 39*	*sphere + horizontal cigar*

Table S4. *Parameters of the CDM models for two periods at Shinmoe-dake and Iwo-yama as given by the maximum a posteriori probability solution with 95% confidence intervals. Depth of the model centroid is reported as below the summit (rounded to the nearest 10 m; and above the mean sea level).* ω_i and $a_i, i = X, Y, Z$ *are the rotation angle (rounded to the nearest 1°; positive for clockwise) and length of the semi-axis along the i-axis (rounded to the nearest 10 m), respectively. Opening is the uniform opening on all three segments. ΔV is the cavity volume change in* 10^3 m^3 *with:* $\Delta V = 4 \cdot (a_X a_Y + a_Y a_Z + a_X a_Z) \cdot \mu$ *for the CDM (Nikkhoo et al., 2016) and* $\Delta V = \Delta P / \mu \cdot \pi r^3$ *for the finite sphere (McTigue, 1987), where μ is the opening and r is the radius.* [#]*not-converged parameters.*

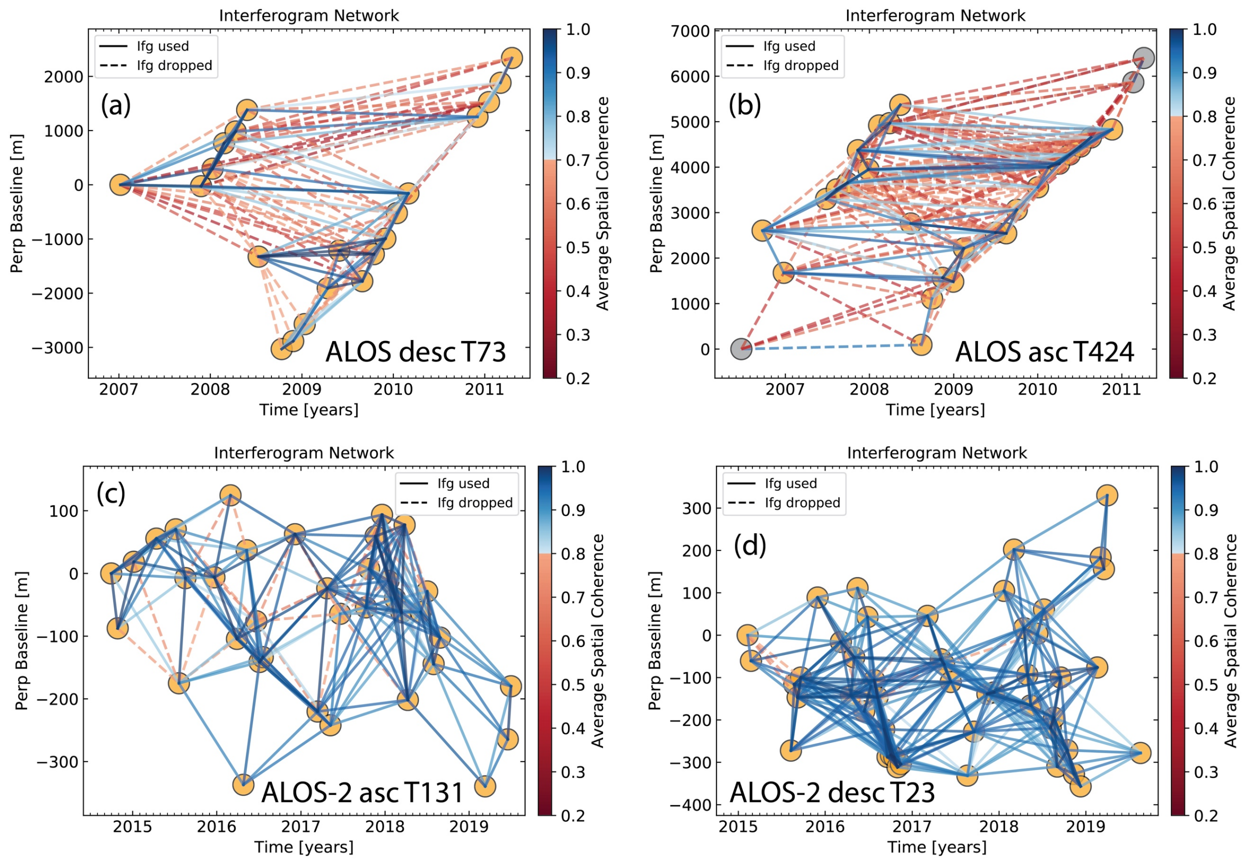

Figure S1. *Network configurations of interferograms stacks. Line colors represent the average spatial coherence of the interferogram calculated over the area of interest around Shinmoe-dake (marked by black squares in Fig. S2). Dashed lines represent the interferograms excluded during the time-series analysis due to low coherence.*

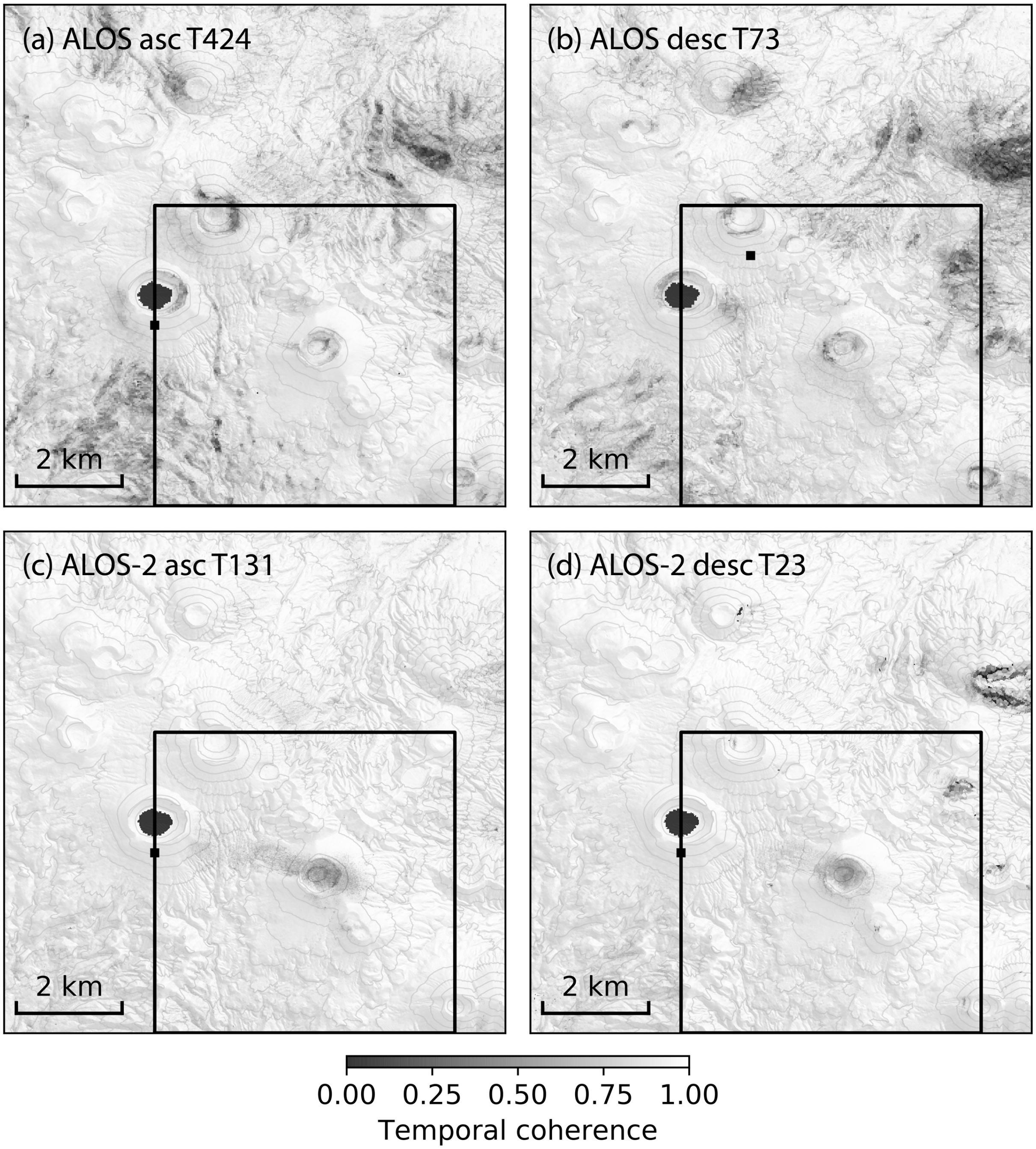

Figure S2. *Temporal coherence of all four datasets from the routine MintPy workflow. Black squares: the custom area of interest used for the coherence-based network modification (Fig. S1).*

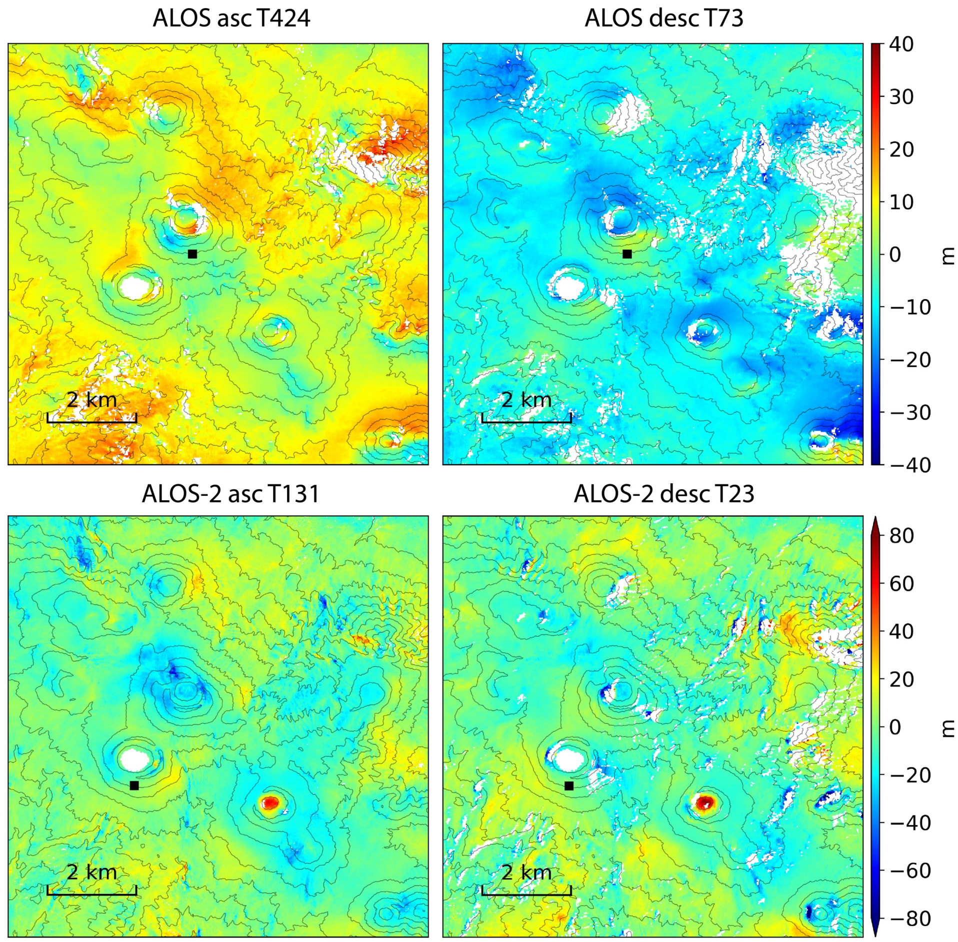

Figure S3. *Estimated DEM error of all four datasets based on the method by Fattahi & Amelung (2013) from acquisitions before the 2011 and 2017 eruptions. Black squares: reference points. Contour lines in every 100 m. In the ALOS-2 estimates, the 60-80 m DEM error at Shinmoe-dake crater represents the lava dome generated from the 2011 eruption. In the ALOS estimates, the opposite sign of the DEM error (+/- 10 m on average) between the ascending and descending orbits reflects a horizontal shift between the coregistered SLC stack and the DEM. Since the same DEM is used for all datasets and the ALOS-2 estimates are normal as expected, we believe this horizontal shift is originated from the ALOS coregistered SLC stack due to improper geometry handling of the ISCE-2 software during SAR focusing. Possible causes include inaccurate starting range re-estimation during the range padding of the native-doppler focusing, inaccurate time tag (only to the closest millisecond), assumption in the focusing of no hidden offset in azimuth, transmit and receive time misuse. Nevertheless, this shift should not affect the displacement time-series after the DEM error correction.*

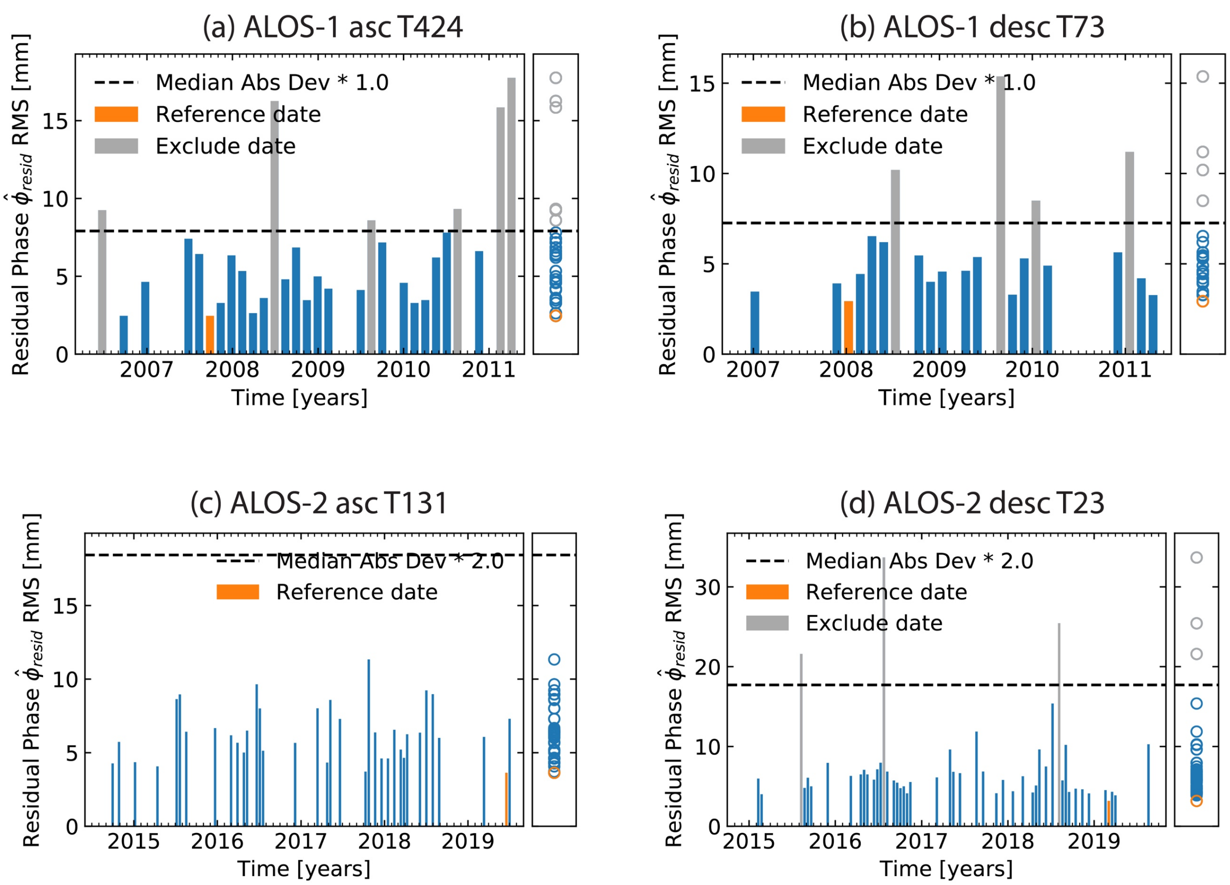

Figure S4. *Residual phase root mean squares (RMS) time-series with noisy acquisitions. The orange bar indicates the acquisition with minimum residual phase RMS and the optimal reference date for each dataset. The gray bars indicate acquisitions with residual phase RMS larger than the predefined threshold (dashed black lines), thus, considered as noisy and excluded during the average velocity estimation.*

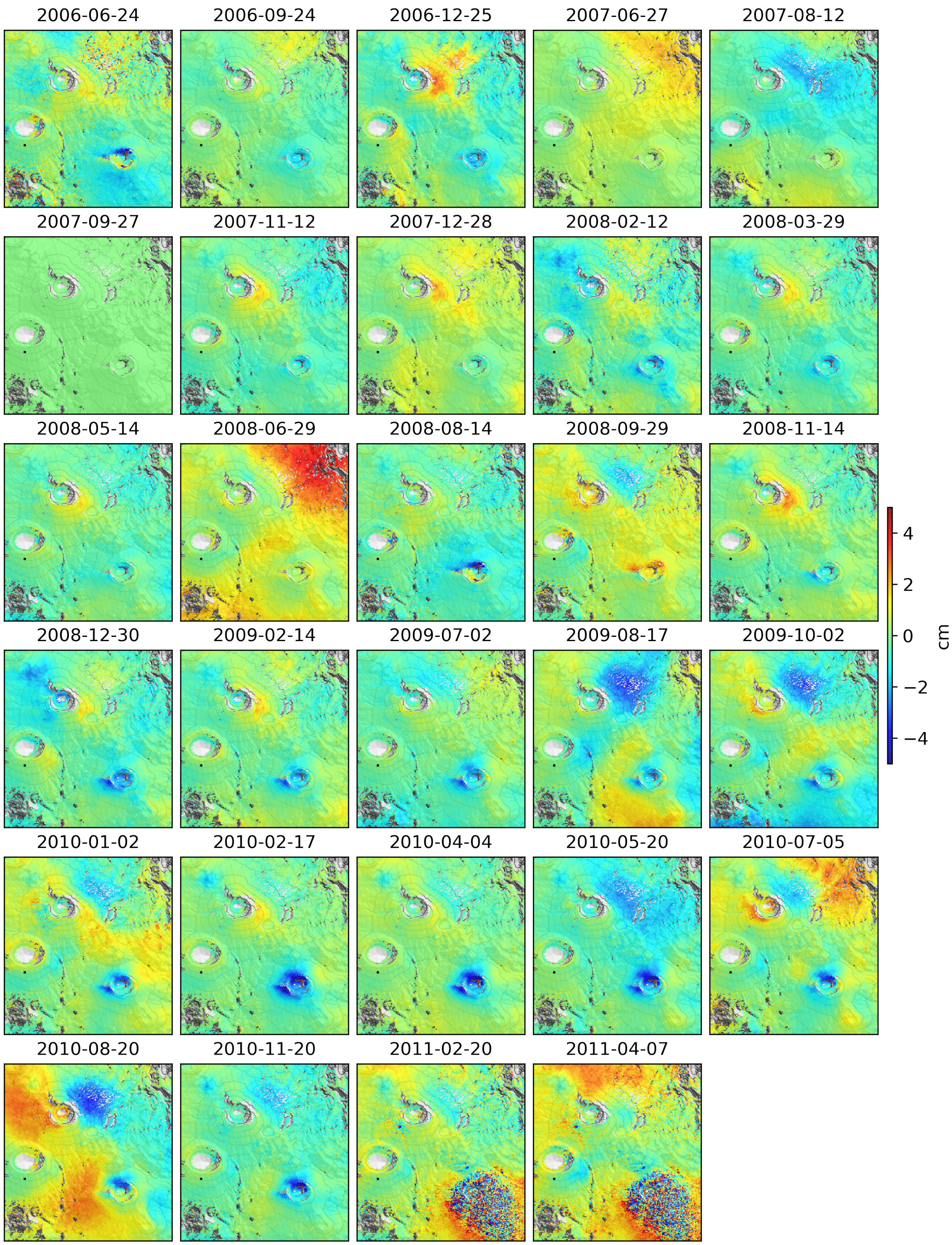

Figure S5. *LOS displacement time-series of Kirishima from ALOS ascending track 424. Positive value for motion toward the satellite. Data are wrapped into [-5, 5) cm for display. Black squares: reference points. Contour lines in every 100 m.*

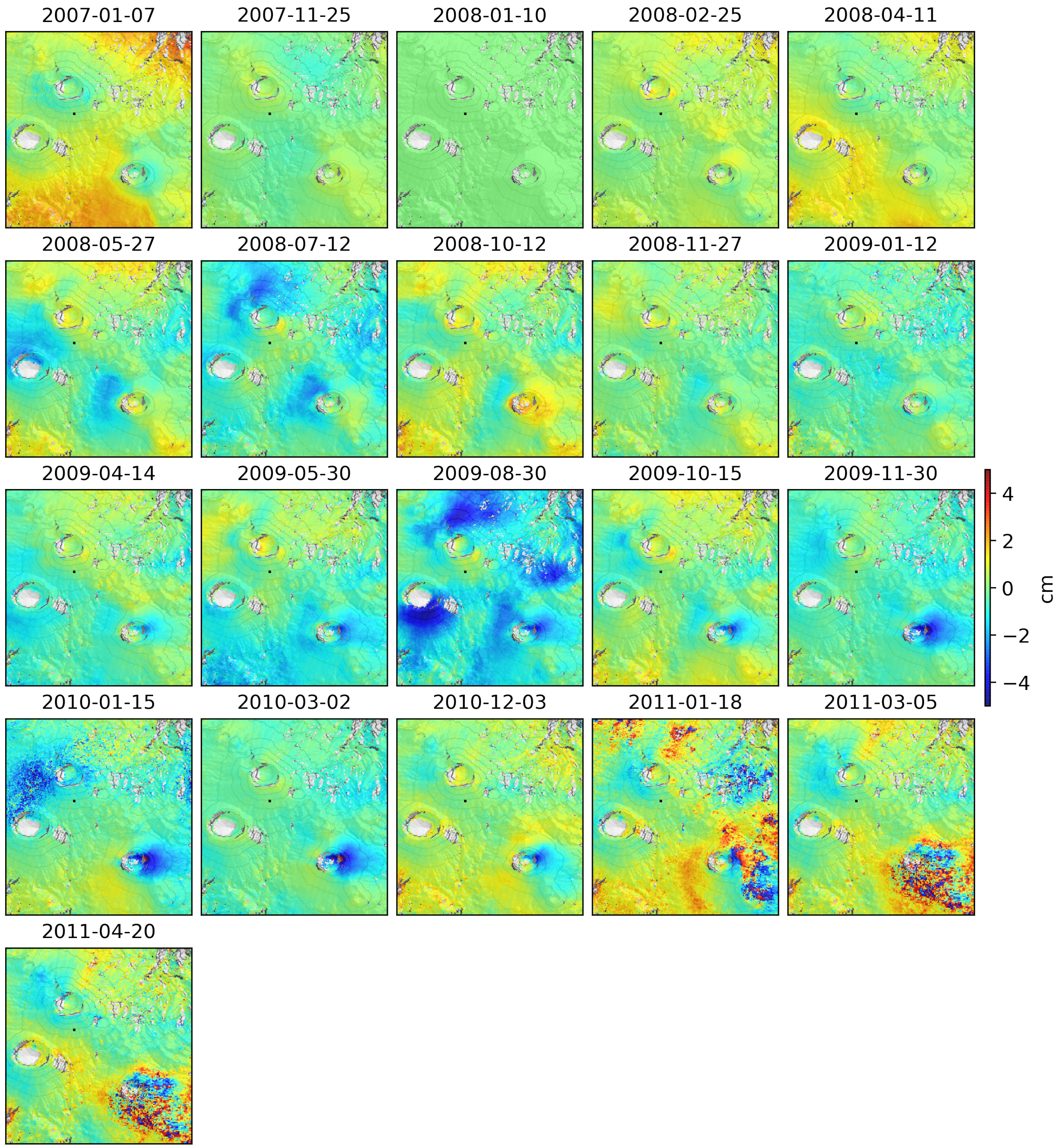

Figure S6. *LOS displacement time-series of Kirishima from ALOS descending track 73. Positive value for motion toward the satellite. Data are wrapped into [-5, 5) cm for display. Black squares: reference points. Contour lines in every 100 m.*

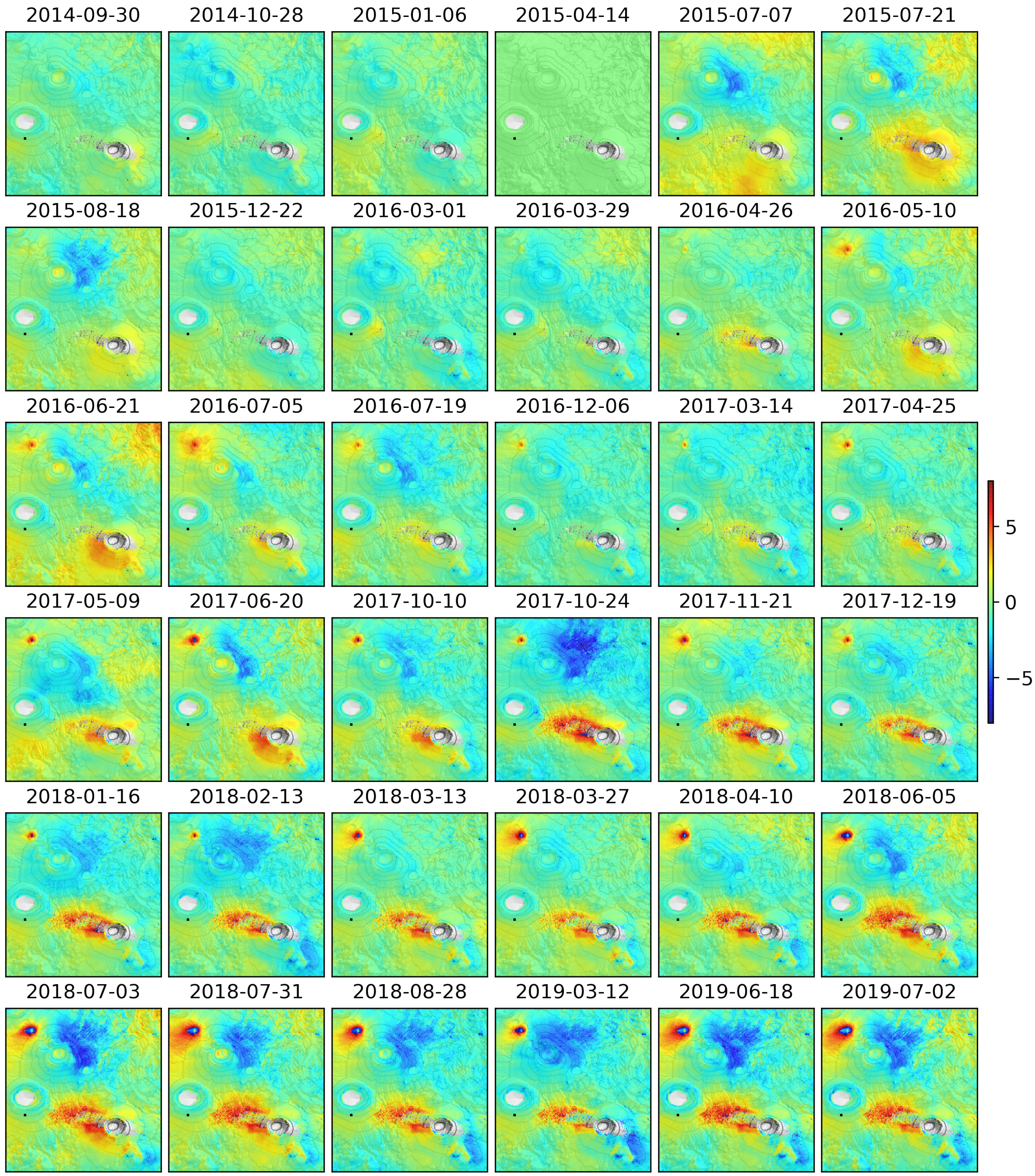

Figure S7. *LOS displacement time-series of Kirishima from ALOS-2 ascending track 131. Positive value for motion toward the satellite. Data are wrapped into [-8, 8) cm for display. Black squares: reference points. Contour lines in every 100 m.*

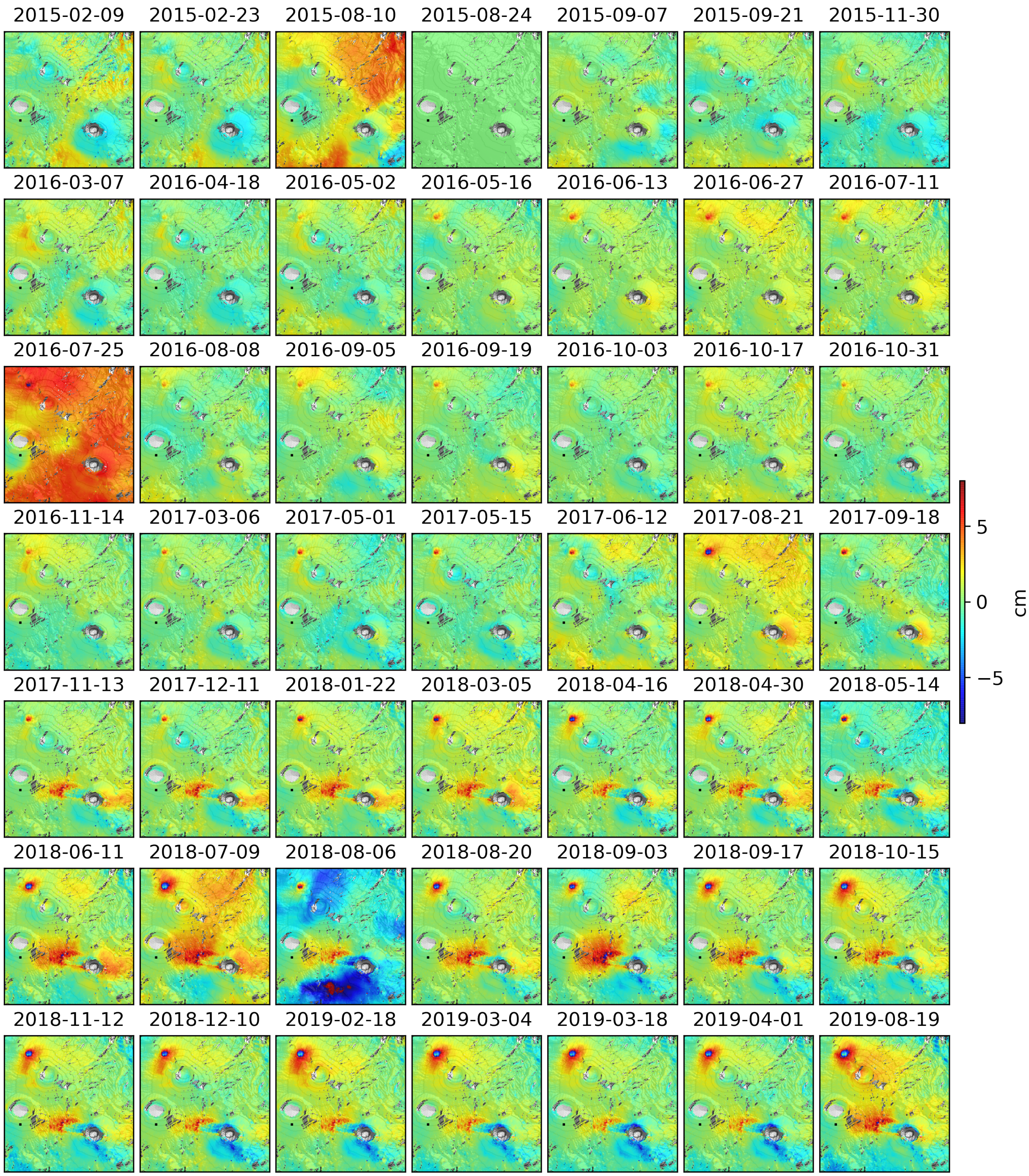

Figure S8. *LOS displacement time-series of Kirishima from ALOS-2 descending track 23. Positive value for motion toward the satellite. Data are wrapped into [-8, 8) cm for display. Black squares: reference points. Contour lines in every 100 m.*

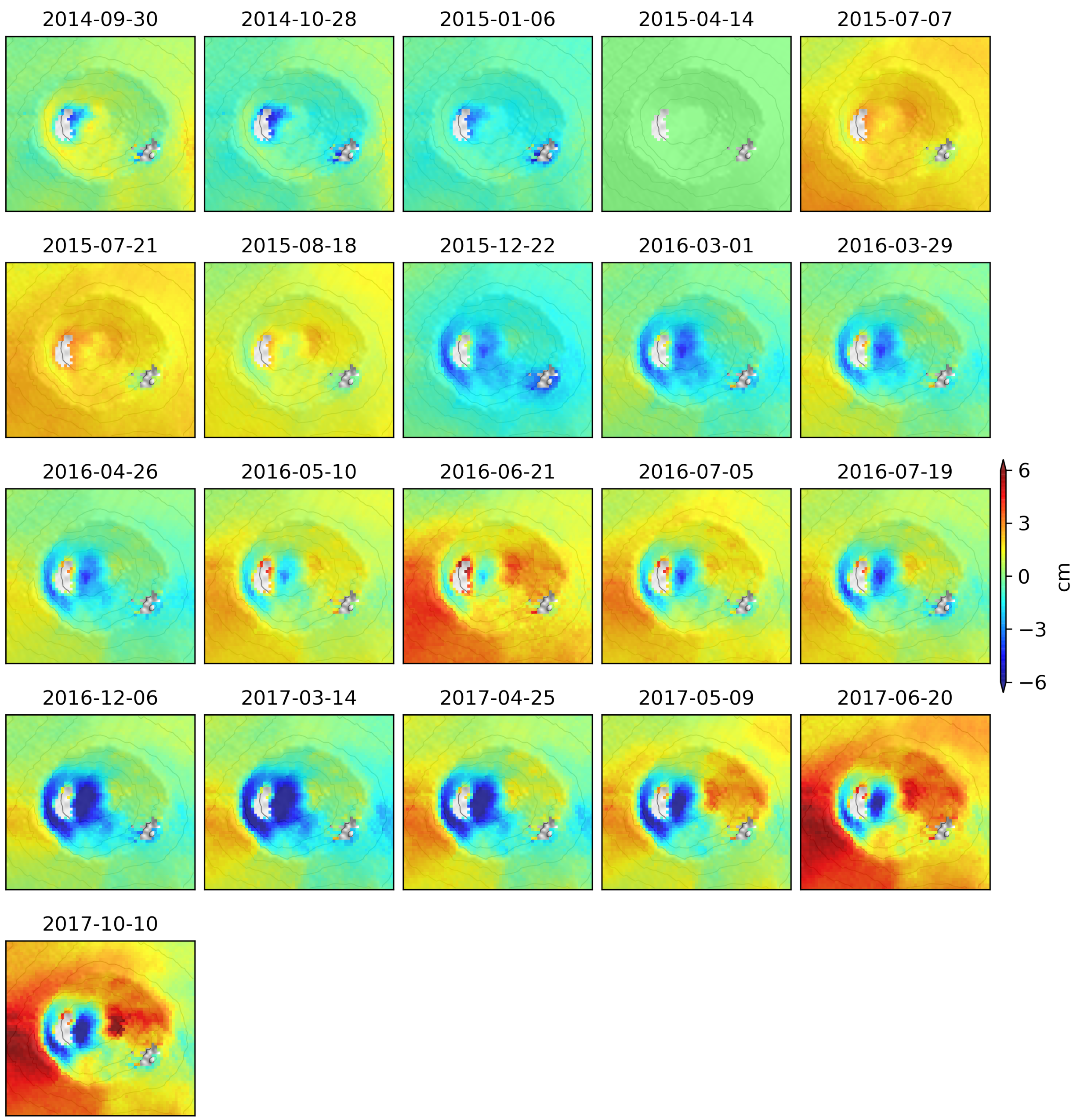

Figure S9. *LOS displacement time-series of Shinmoe-dake crater [E130.877º - E130.889º, N31.906º - N31.917º] before the October 2017 eruption from ALOS-2 ascending track 131. Positive value for motion toward the satellite. Contour lines in every 50 m. Reference point is outside of the map extent (E130.877º - E130.889º, N31.906º - N31.917º) at [E130.894º, N31.921º].*

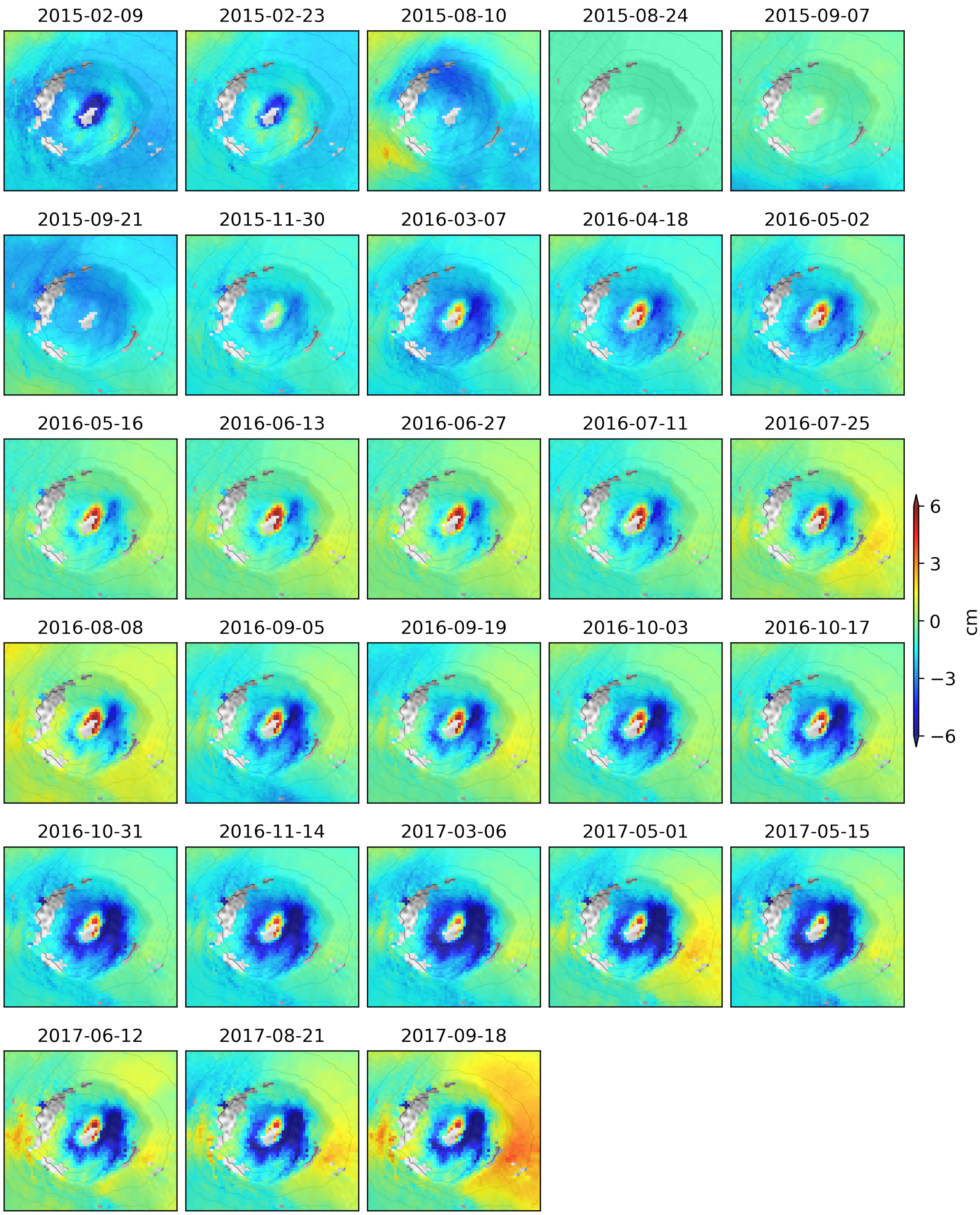

Figure S10. *LOS displacement time-series of Shinmoe-dake crater before the October 2017 eruption from ALOS-2 descending track 23. Positive value for motion toward the satellite. Contour lines in every 50 m. Reference point is outside of the map extent (E130.877º - E130.889º, N31.906º - N31.917º) at [E130.894º, N31.921º].*

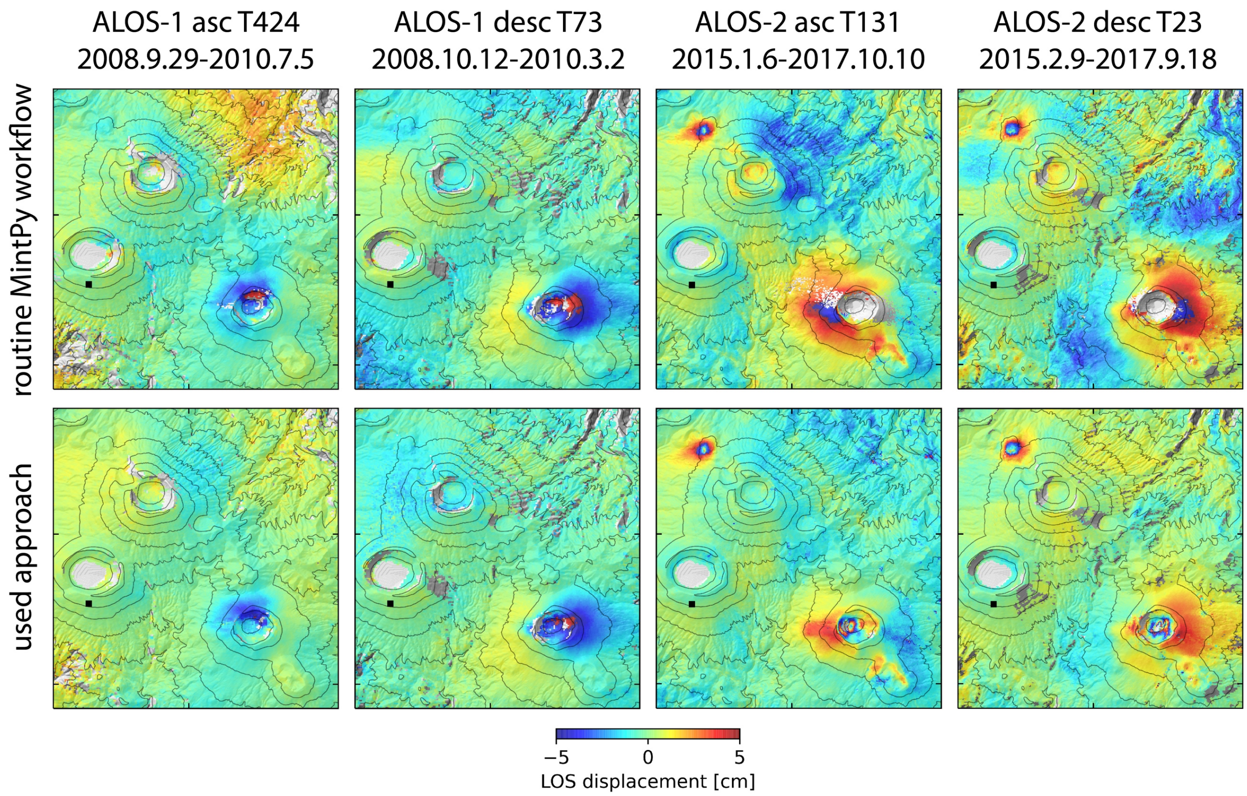

Figure S11. *Comparison between two approaches to estimate LOS displacements. Top panel: differential displacements between two acquisitions from displacement time-series using the routine MintPy workflow. Bottom panel (used approach): displacements converted from the linear velocity of the time periods of interest, estimated from the displacement time-series after additional network modification by excluding interferograms with acquisitions after the 2011 and 2017 eruptions. Positive value for motion toward the satellite. Contour lines in every 100 m.*

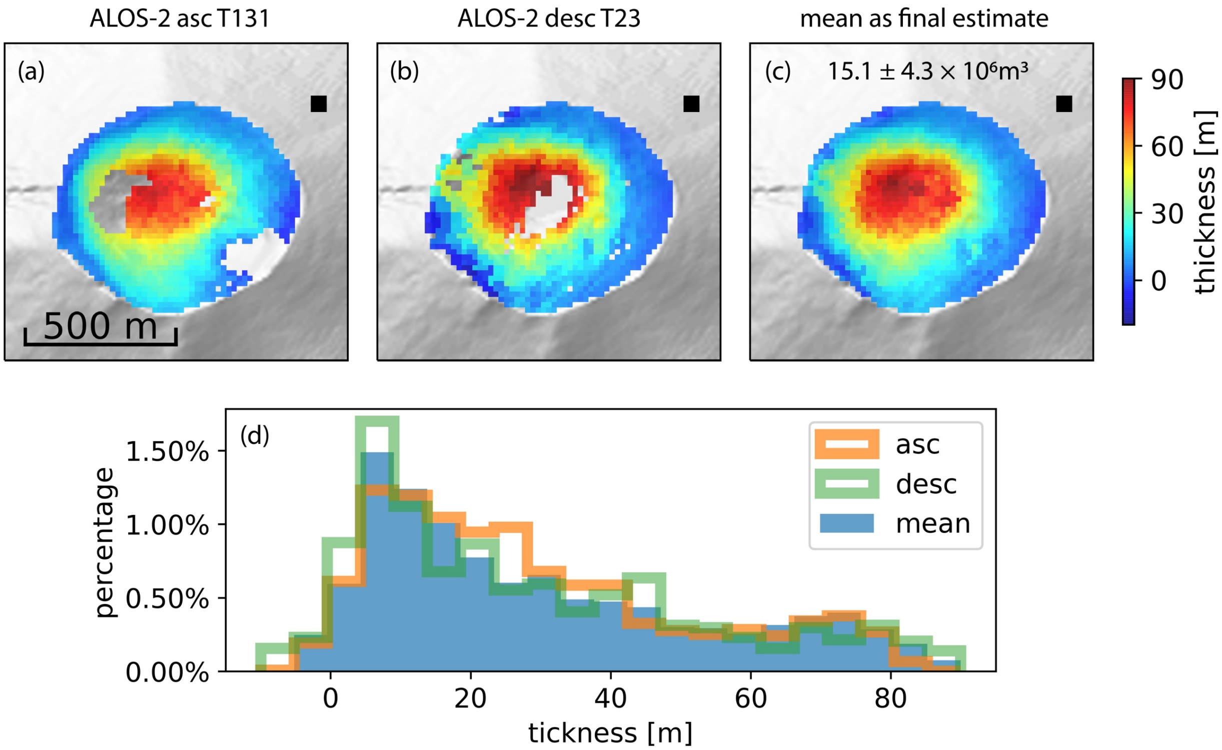

Figure S12. *Lava dome thickness at the Shinmoe-dake crater due to the 2011 eruption estimated from the ALOS-2 DEM error estimates (Fig. S3 lower panel). (a-b) Thickness estimates from ALOS-2 ascending and descending orbits, respectively. (c) Average of (a-b). (d) Histogram of (a-c). We use a common local reference point (black square) to align the relative DEM error to the Shinmoe-dake crater. A high temporal coherence threshold (0.95) is used to discard noisy pixels, resulting in the masked-out areas in (a-b). Both ascending and descending estimates are used to get the mean estimate and fill the masked-out areas. The remaining masked-out areas (4 pixels) are filled with the nearest data. The estimated volume of the lava dome is* $15.1 \pm 4.3 \times 10^6 m^3$ *with three-sigma intervals. This estimate is similar to Ozawa & Kozono (2013;* $15.4 \times 10^6 m^3$*) using SAR intensity simulation from TerraSAR-X image of 1 February 2011, but lower than Shimono et al. (2011;* $19 \times 10^6 m^3$*) using single-pass SAR interferometry from airborne SAR data of 7 February 2011.*

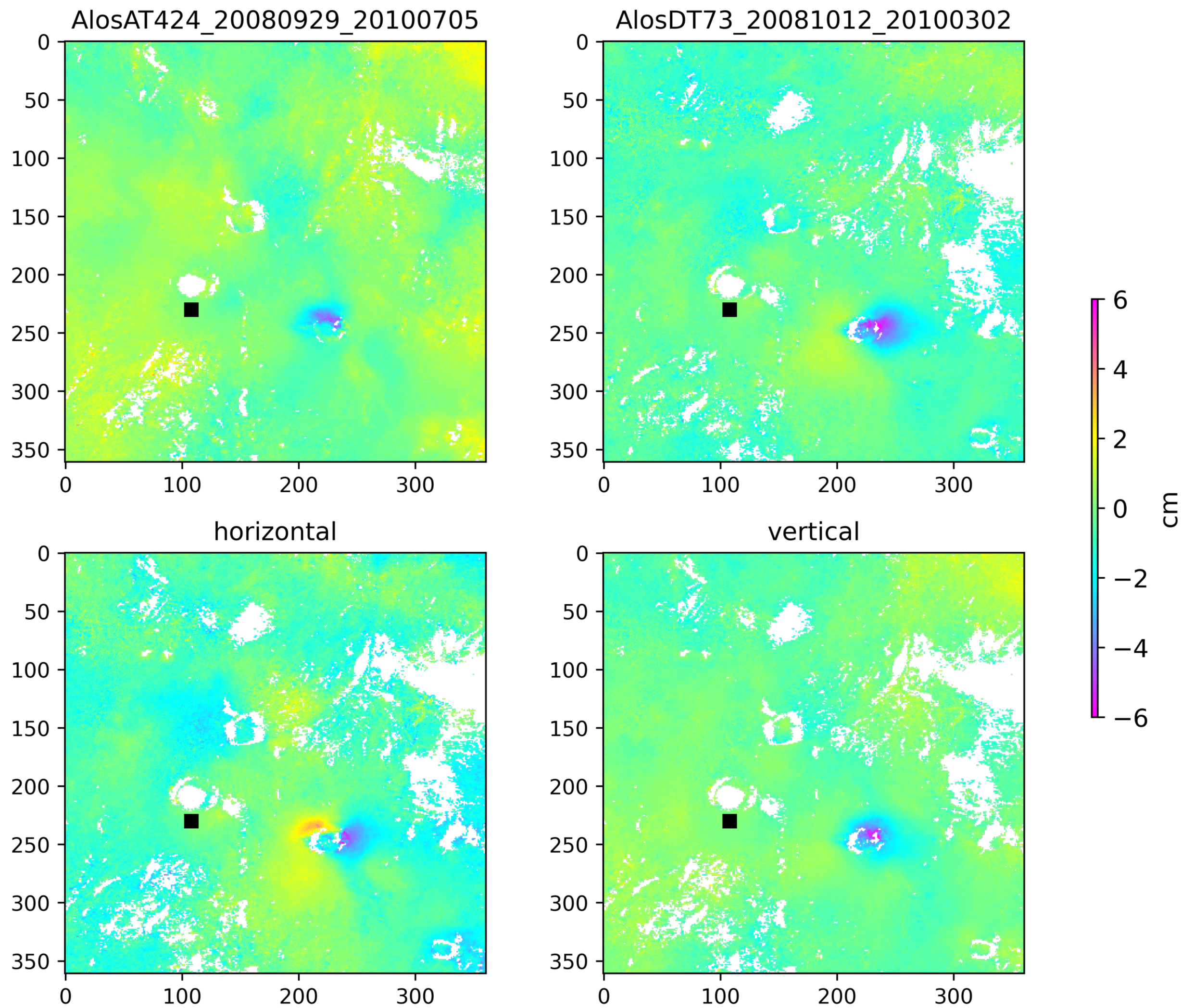

Figure S13. *Deflation at Shinmoe-dake during the 2008-2010 eruptions. Top panel: LOS displacement from ALOS ascending track 424 and descending track 73, respectively. Positive value for motion toward the satellite. Bottom panel: quasi-east-west and quasi-vertical displacement decomposed from the top panel. Positive value for motion toward the east and uplift. Data are wrapped into [-6, 6) cm for display. Related to Fig. 1d.*

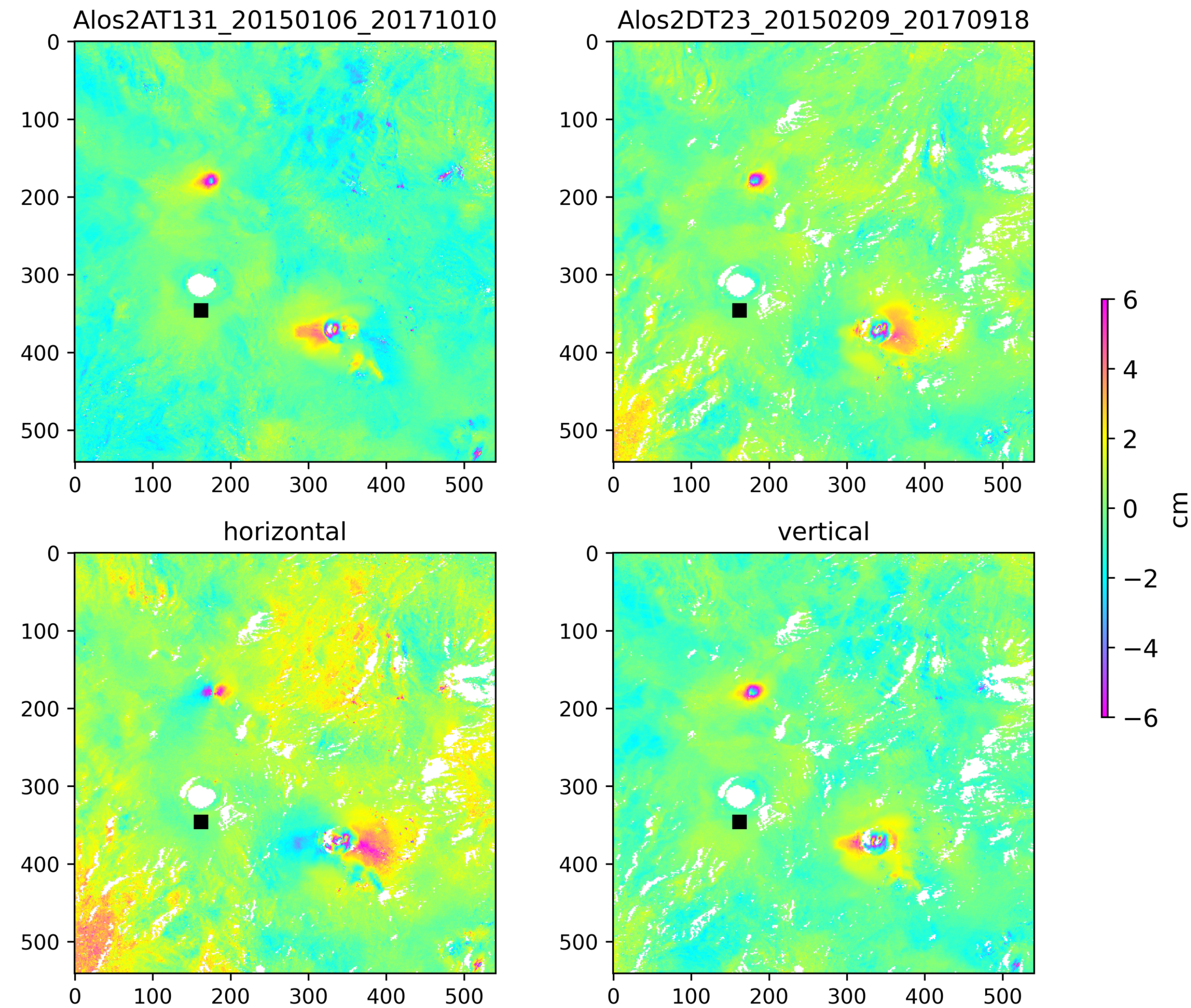

Figure S14. *Inflation at Shinmoe-dake and Iwo-yama before the October 2017 eruption. Top panel: LOS displacement from ALOS-2 ascending track 131 and descending track 23, respectively. Positive value for motion toward the satellite Bottom panel: quasi-east-west and quasi-vertical displacement decomposed from the top panel. Positive value for motion toward the east and uplift. Data are wrapped into [-6, 6) cm for display. Related to Fig. 1e.*

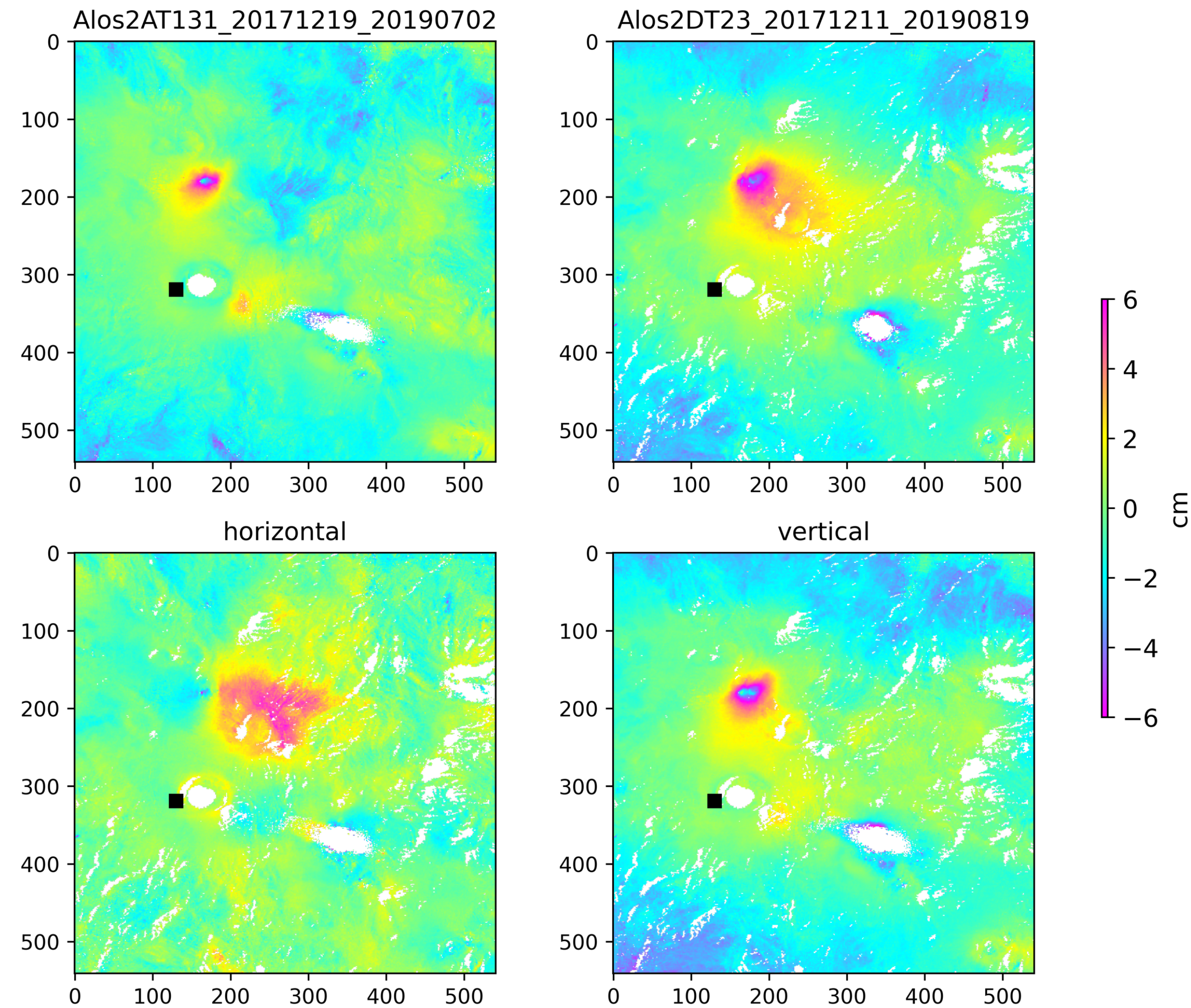

Figure S15. *Deflation at Shinmoe-dake and inflation at Iwo-yama after December 2017. Top panel: LOS displacement from ALOS-2 ascending track 131 and descending track 23, respectively. Positive value for motion toward the satellite. Bottom panel: quasi-east-west and quasi-vertical displacement decomposed from the top panel. Positive value for motion toward the east and uplift. Data are wrapped into [-6, 6) cm for display. Related to Fig. 1f.*

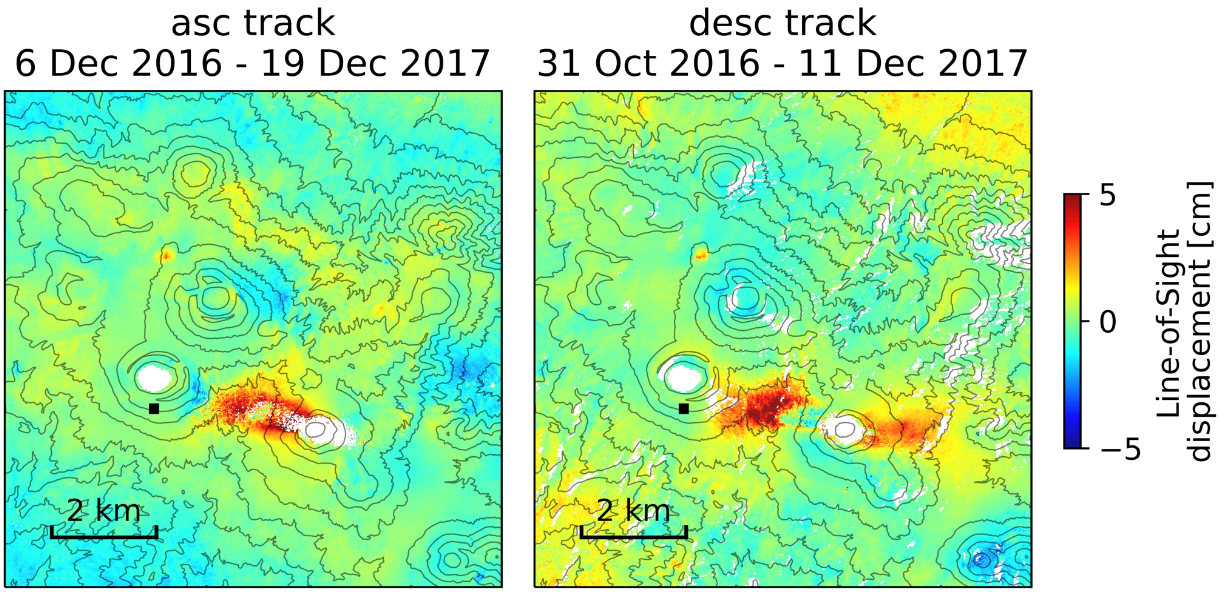

Figure S16. *Ash/tephra deposition from the October 2017 Shinmoe-dake eruption. Left and right: ALOS-2 ascending track 131 and descending track 23, respectively. Positive values indicate motion toward the satellite. Black squares: reference points. Contour lines in 100 m.*

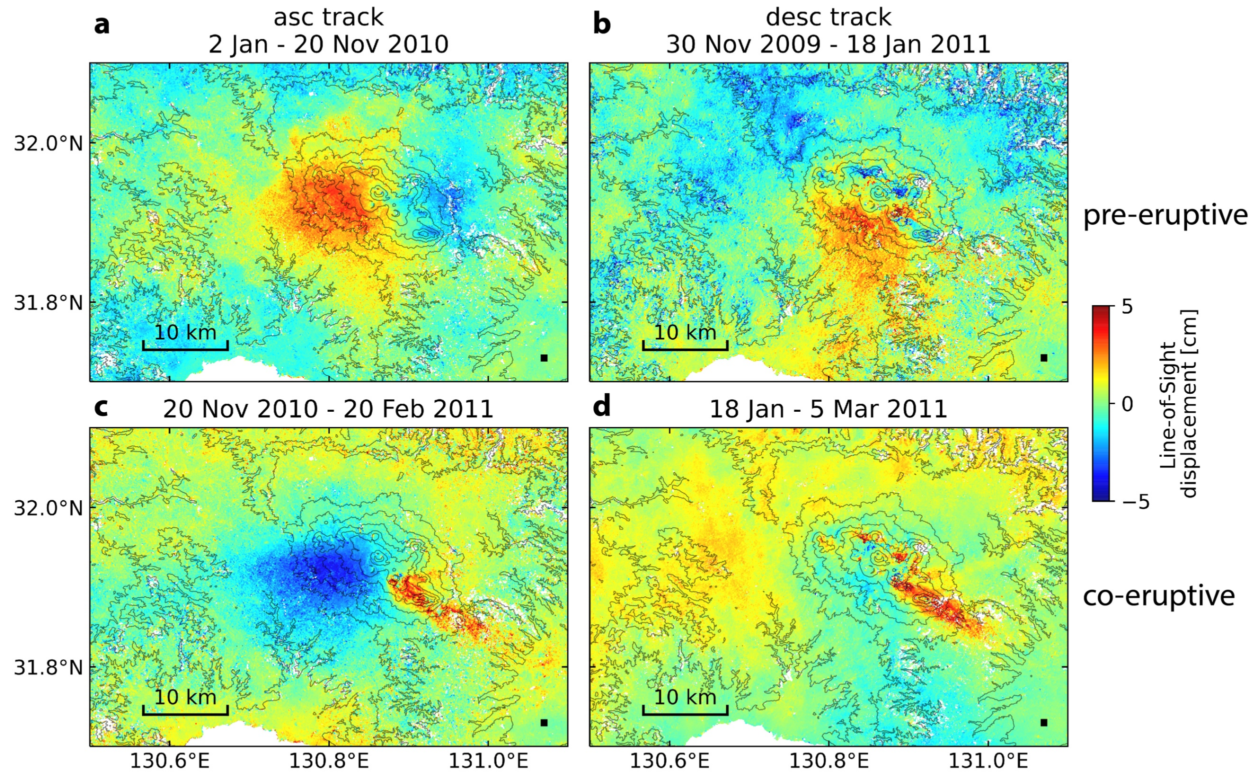

Figure S17. *Pre-/co-eruptive deformation of the 2011 Shinmoe-dake eruption. Left and right: ALOS ascending track 424 and descending track 73, respectively. Positive values indicate motion toward the satellite. Black squares: reference points. Contour lines in 200 m. Red long tail pattern in (c-d): ash/tephra deposition from the eruption.*

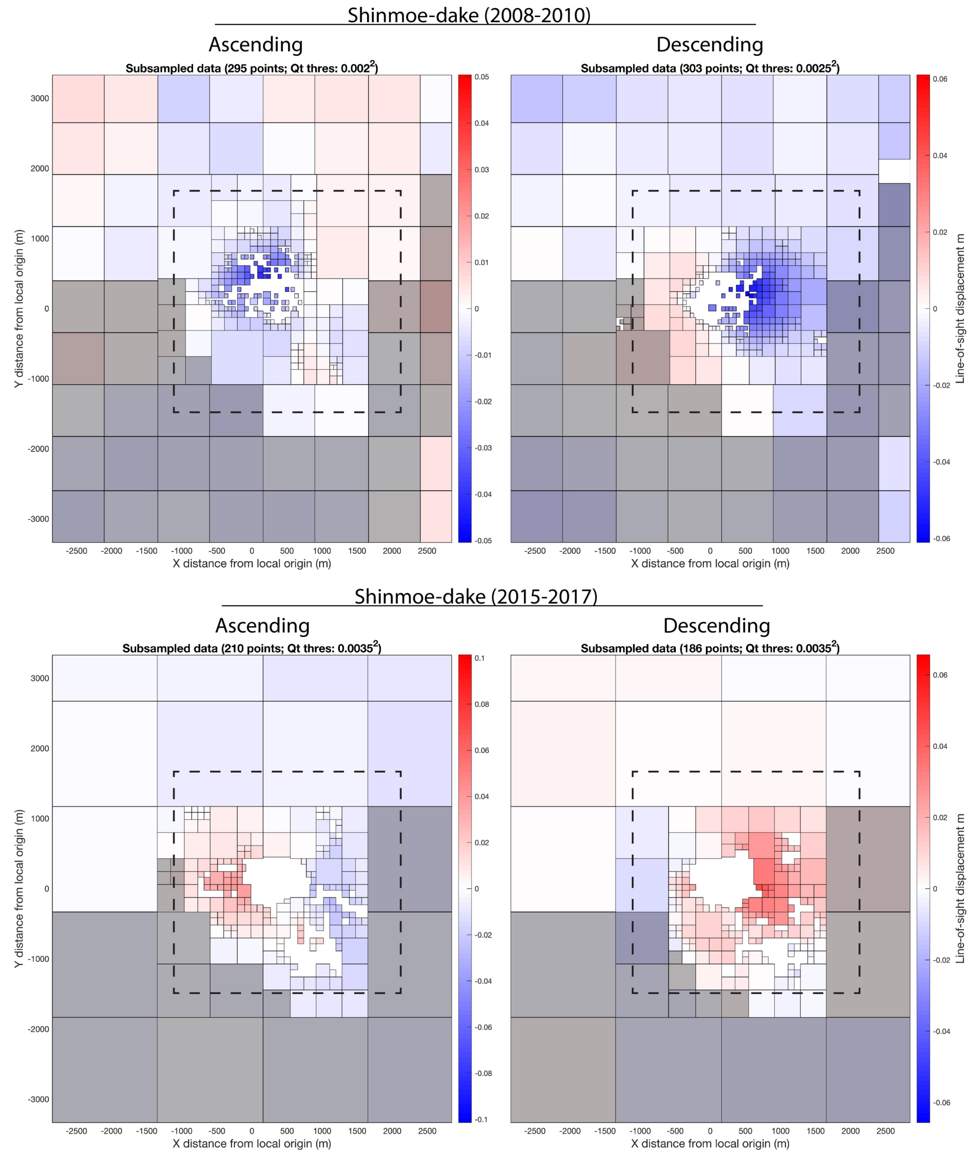

Figure S18. *Subsampled LOS displacement at Shinmoe-dake from ALOS and ALOS-2 ascending and descending orbits. Positive value for motion toward the satellite. Black dashed rectangle represents Fig. 3a-i coverage. We apply a minimum free surface height constraint of 1,100 m (shaded grids). This affects 74 (with an average / min / max height increase of 119 / 7 / 343 m) out of 598 points (12%) for the 2008-2010 period; and 30 (with an average / min / max height crease of 82 / 1 / 273 m) out of 396 points (8%) for the 2015-2017 period.*

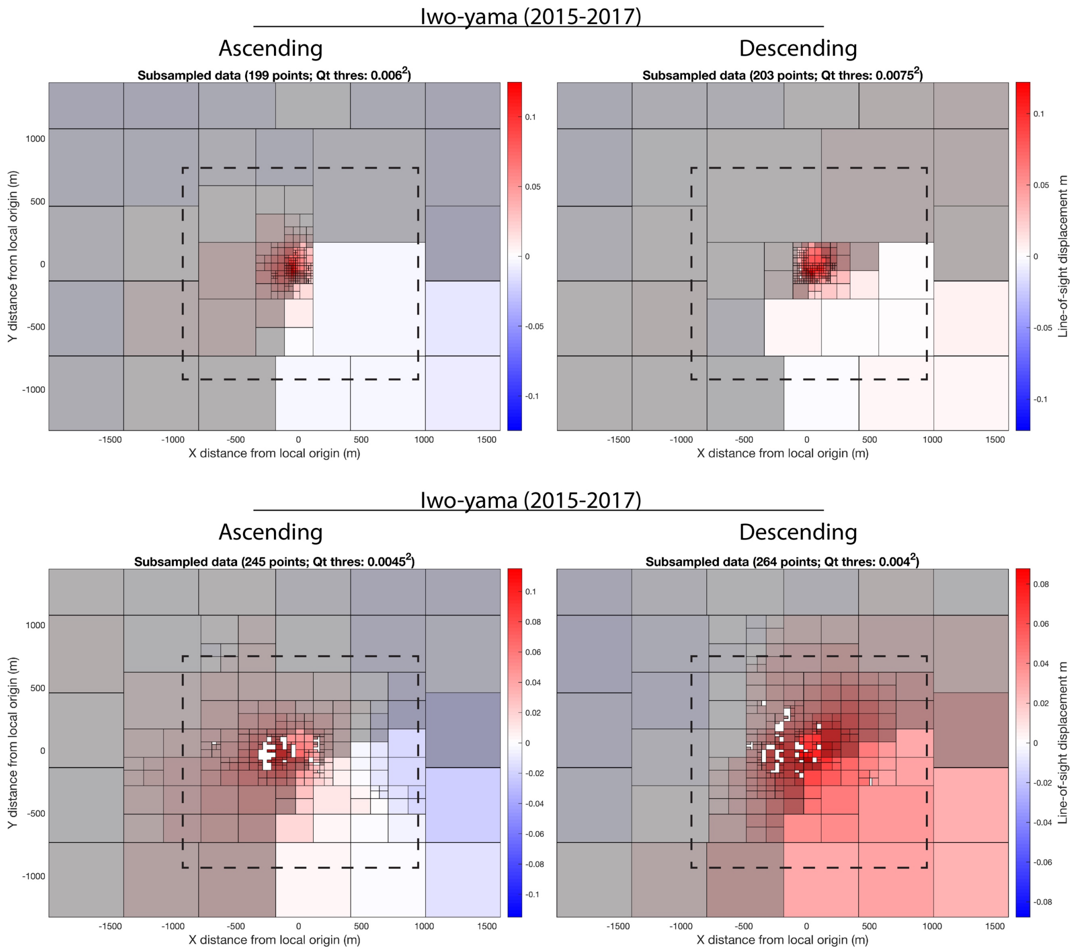

Figure S19. *Subsampled LOS displacement data at Iwo-yama from ALOS-2 ascending and descending orbits. Positive value for motion toward the satellite. Black dashed rectangle represents Fig. 3k-s coverage. We apply a minimum free surface height constraint of 1,300 m (shaded grids). This affects 239 (with an average / min / max height increase of 32 / 0 / 287 m) out of 402 points (59%) for the 2015-2017 period; and 394 (with an average / min / max height crease of 56 / 0 / 287 m) out of 509 points (77%) for the 2017-2019 period.*

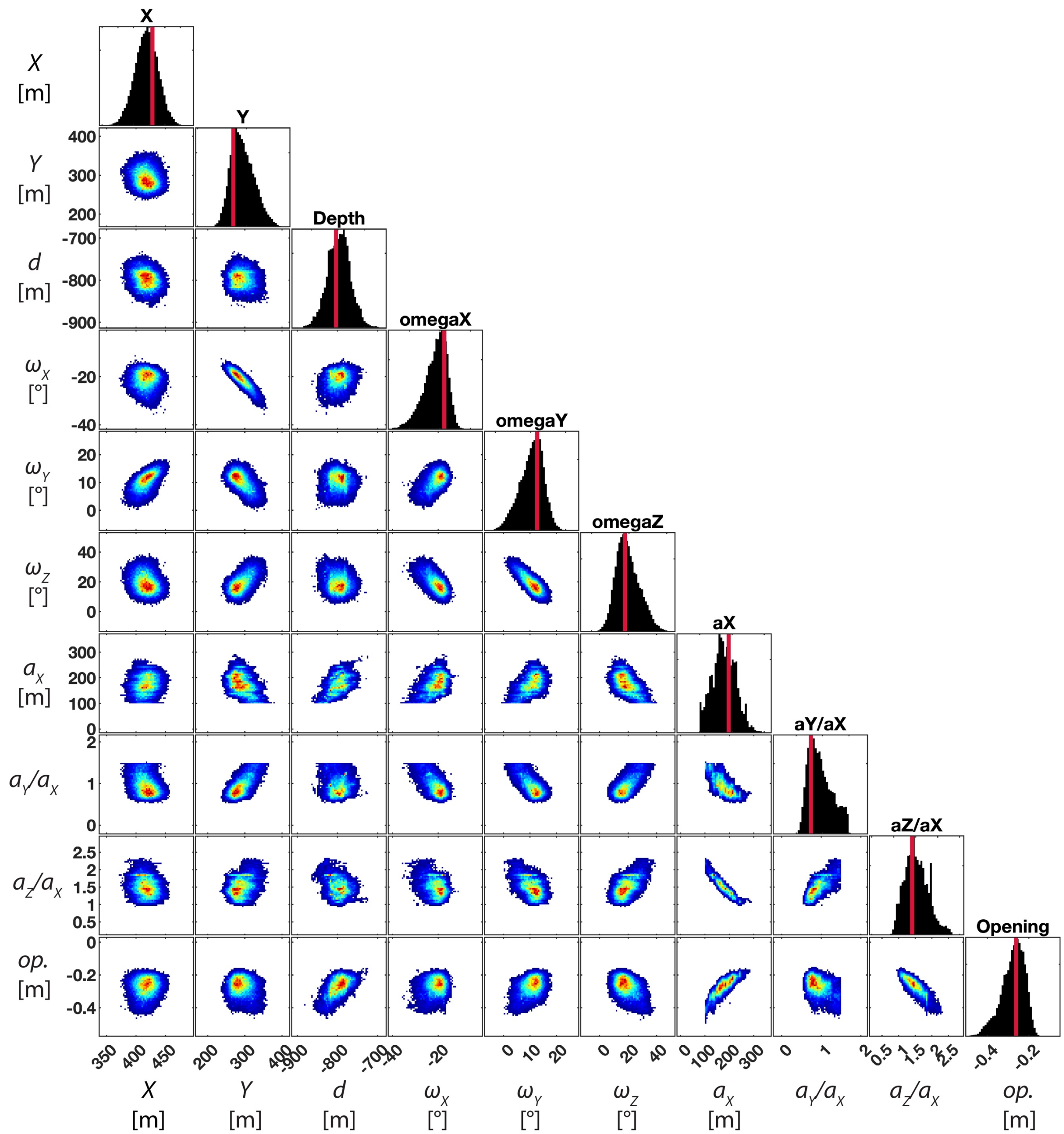

Figure S20. *Marginal posterior probability distributions of the CDM parameters for the deflation between the 2008-2010 phreatic eruptions at Shinmoe-dake. Black bars in the diagonal: posterior probability distribution for each parameter. Red lines: maximum a posteriori probability (optimal) solution.* $\boldsymbol{\omega_i}$ ***and*** $\boldsymbol{a_i}, \boldsymbol{i = X, Y, Z}$ *are the rotation angle (positive for clockwise) and length of the semi-axis along the i-axis, respectively. Related to Fig. 2a-e.*

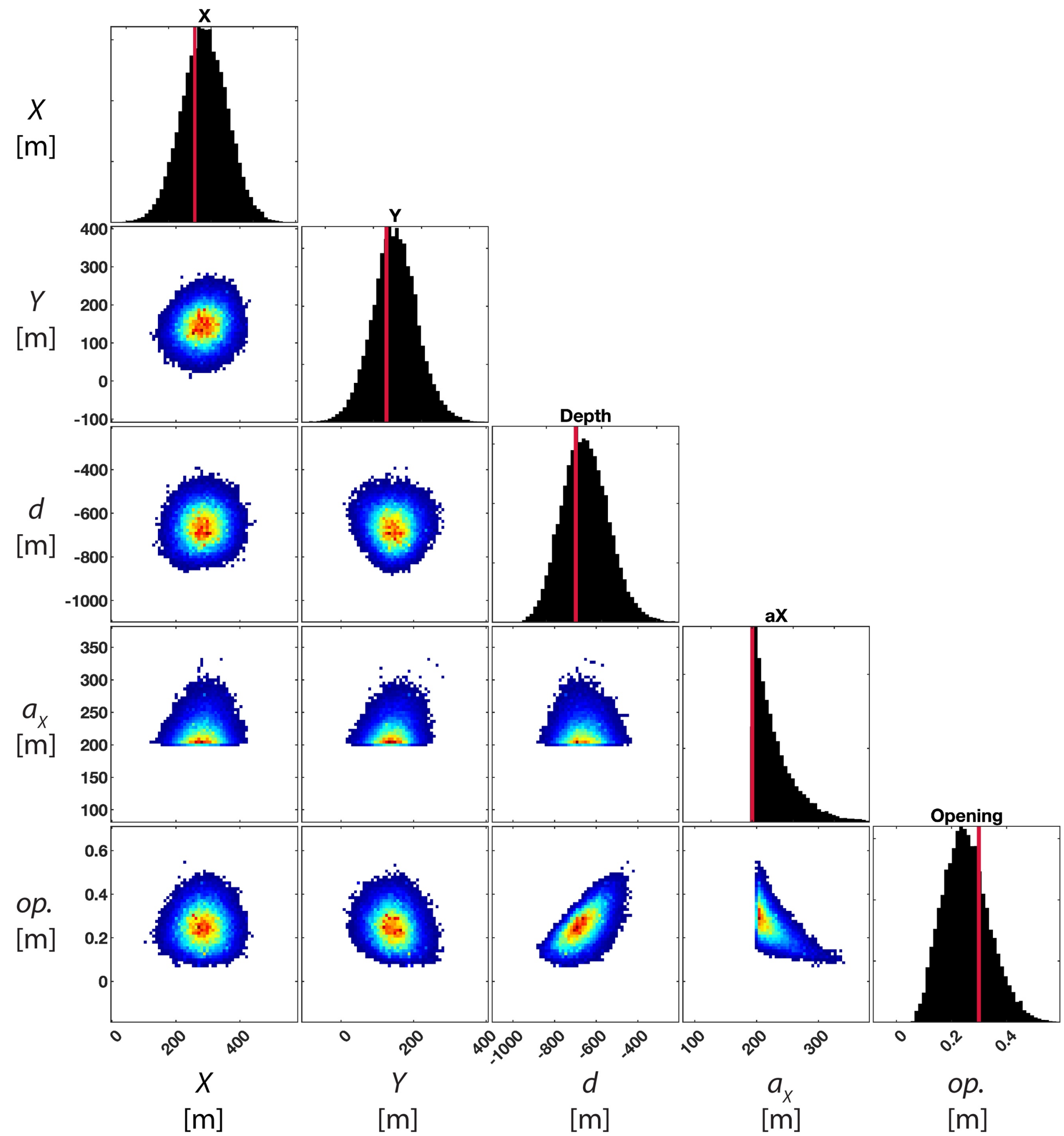

Figure S21. *Marginal posterior probability distributions of CDM parameters for the pre-eruptive inflation of the 2017 magmatic eruption at Shinmoe-dake. Fixed parameters are not shown. Black bars in the diagonal: posterior probability distribution for each parameter. Red lines: maximum a posteriori probability (optimal) solution. Related to Fig. 2f-j.*

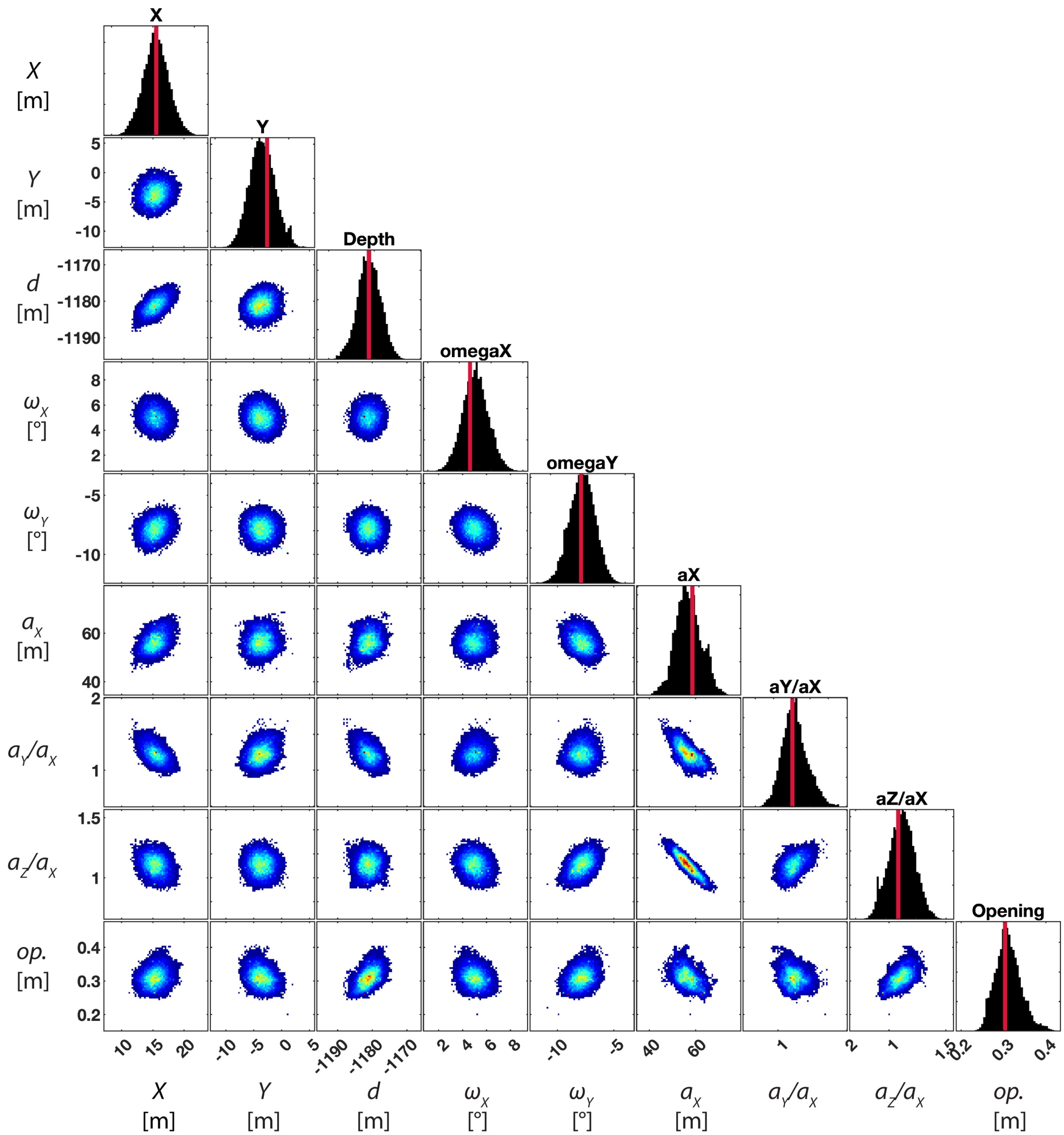

Figure S22. *Marginal posterior probability distributions of CDM parameters for the inflation before October 2017 at Iwo-yama. Fixed parameters are not shown. Black bars in the diagonal: posterior probability distribution for each parameter. Red lines: maximum a posteriori probability (optimal) solution. Related to Fig. 2k-o.*

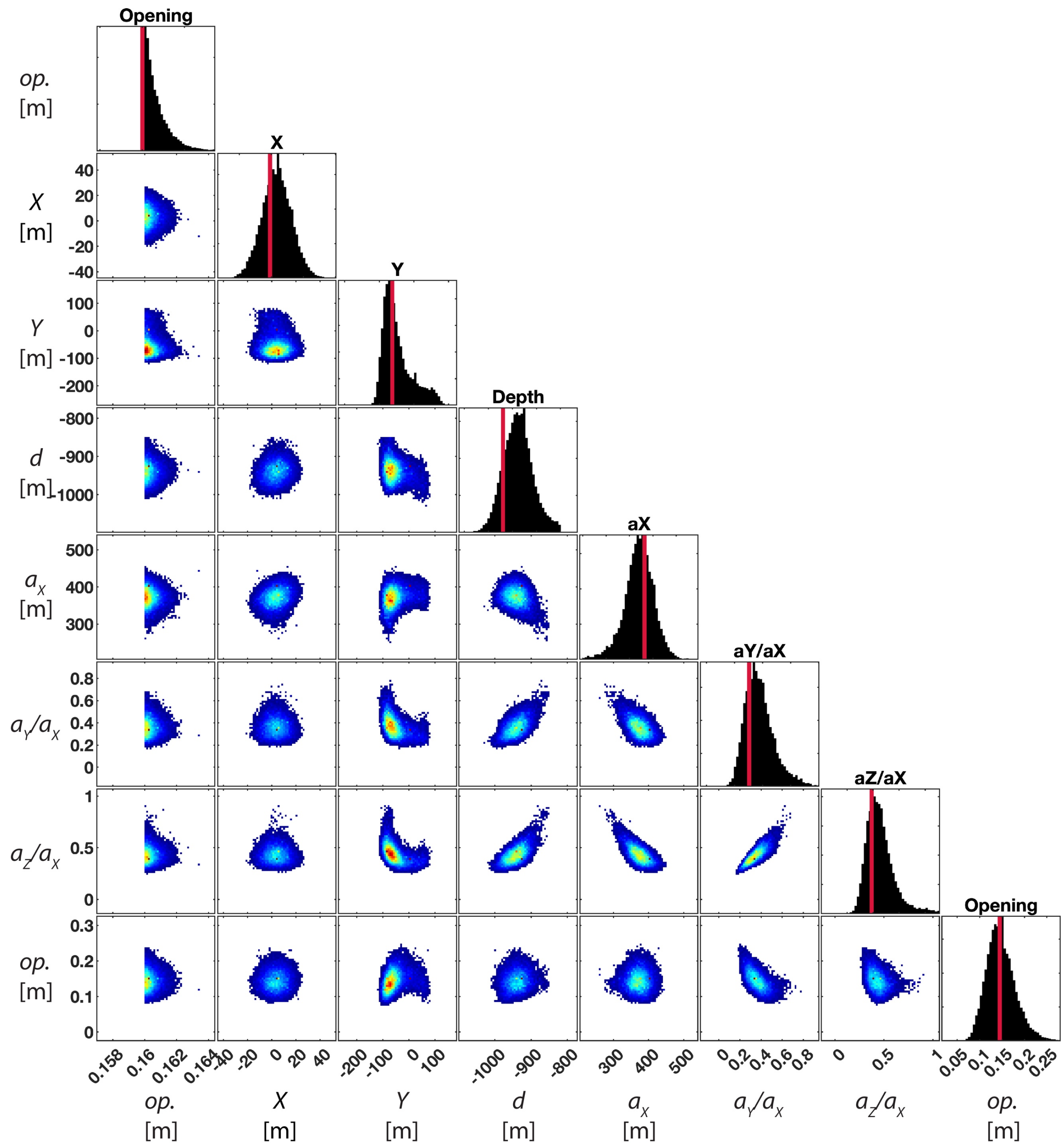

Figure S23. *Marginal posterior probability distributions of two CDMs parameters for the expanded inflation after December 2017 at Iwo-yama. Fixed parameters are not shown. Black bars in the diagonal: posterior probability distribution for each parameter. Red lines: maximum a posteriori probability (optimal) solution. Related to Fig. 2p-t.*

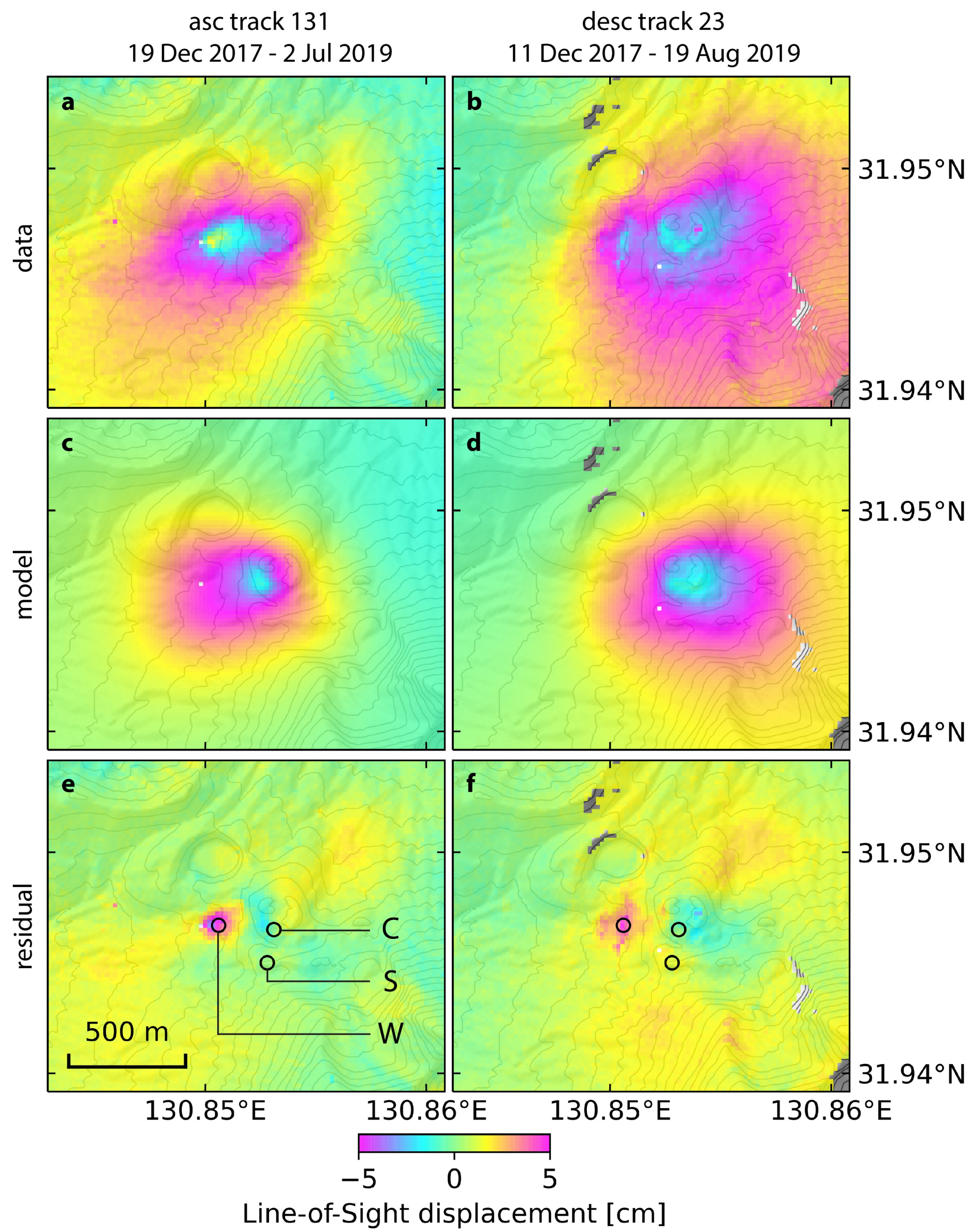

Figure S24. *Residual between the observed and predicted displacement from two CDMs at Iwo-yama after December 2017. Contour lines in 20 m. Point C, S and W are the same as in Fig. 1. Positive values for motion toward the satellite. Related to Fig 1g and 2p-t.*